ELSEVIER

Chemical Engineering Journal 82 (2001) 73–85

Chemical Engineering Journal

www.elsevier.com/locate/cej

# Improved-performance knitted fibre mats as supports for pre-mixed natural gas catalytic combustion

I. Cerri [a], G. Saracco [a,*], V. Specchia [a], D. Trimis [b]

[a] *Dipartimento di Scienza dei Materiali ed Ingegneria Chimica, Politecnico di Torino, Corso Duca degli Abruzzi 24, 10129 Torino, Italy*
[b] *Institute of Fluid Mechanics, University of Erlangen-Nuremberg, Cauerstr. 4, D-91058 Erlangen, Germany*

Received 1 June 2000; accepted 7 October 2000

**Abstract**

As an improvement of previously developed catalytic burners based on $LaMnO_3$ catalysts deposited on a FeCrAl alloy fibre mat (NIT100s by ACOTECH BV), new catalytic burners have been developed showing improved catalytic activity and sulphur resistance, a prevalent issue to be addressed owing to the presence of odorants (e.g. THT) in the natural gas distributed in the network. Such properties are entailed by adoption of new catalysts ($LaMnO_3 + 17MgO$) developed on purpose, where the presence of MgO acts both as a structural promoter (reducing the average grain size of the perovskite catalyst by nearly one order of magnitude) and a sulphur-poisoning preventing agent (by selectively reacting with $SO_2$ originated from the combustion of the odorant). The performance of the new catalytic burner is compared in this paper to those of the non-catalytic burner and the previously developed $LaMnO_3$-catalysed burner in both fresh and aged status as a function of the prevalent parameters affecting the combustion regime (specific power input $Q$, excess of air $E_a$). Particularly promising results are enlightened at low $Q$ and $E_a$ values ($<250\,kW\,m^{-2}$ and 10%, respectively), where the non-catalytic burner and the aged $LaMnO_3$-catalytic burner entail unacceptable high CO emissions (well exceeding 100 ppmv).

A preliminary mono-dimensional modelling of the combustion in the porous burners including heat, mass and momentum balances in the combustion chamber and a pseudo-homogeneous approach to the description of the behaviour of the porous burner is presented. Model calculations obtained through ad hoc developed code (FASTEST) show just encouraging results that pave the way towards further improvements of the modelling tool. 

*Keywords:* Porous media; Catalytic combustion; $LaMnO_3$ perovskite; MgO; Sulphur poisoning; Combustion modelling

## 1. Introduction

In the last decades, pre-mixed combustion in porous media has received extensive experimental [1,2] and theoretical attention [3–6] especially for its potential in enhancing the efficiency of heat transfer and reducing the environmental impact due to pollutant emissions: the greenhouse gas $CO_2$, the toxic gases CO, $NO_x$ and unburned hydrocarbons (HC). In this technology the fuel/air mixture is fed to a porous panel, where combustion is ignited by sparking and, depending on the operating conditions (specific feed flow rate, excess of air, structure of the combustion chamber), the flame front is stabilised close to the downstream surface of the panel or even partly inside of it. As opposed to free flame technology, porous media combustion allows a stronger heat exchange by radiation and conduction from the solid to the heat sink; this entails both an increase of the thermal efficiency and a reduction of flame temperatures, thereby enabling a lower generation of thermal $NO_x$. As generally recognised, depending on the thermo-physical properties of the porous medium (permeability, emissivity, conductivity, etc.) and on the operating conditions (specific input power $Q$, 200–2000 $kW\,m^{-2}$, and excess air $E_a$, 5–70%), three different regimes can be established: the radiant, the transition and the blue-flame modes [7]. The radiant regime, typically occurring at low $Q$ and $E_a$ values, is characterised by a homogeneously red colour of the burnerdeck, a consequence of the high temperatures reached by the downstream layers of porous material (800–1000°C). Particularly low $NO_x$ emissions are expected in this regime, whereas rather high CO concentrations are often produced at particularly low $Q$ and $E_a$ values. In the blue flame regime, established at high $Q$ and $E_a$ values, a carpet of blue flames covers the porous panel leaving the burner material comparatively cold. Higher $NO_x$ emissions and very low HC and CO emissions are typically encountered in this operating mode compared to its previous counter part. For average $Q$ and $E_a$ values, the burner is characterised by the co-existence of radiating and blue-flames

* Corresponding author. Tel.: +39-11-5644654; fax: +39-11-5644699.
*E-mail address:* saracco@polito.it (G. Saracco).

1385-8947/01/$ – see front matter 
PII: S1385-8947(00)00344-2

**Nomenclature**

| | |
|---|---|
| $A$ | reactant |
| $B$ | product |
| $c$ | molar concentration (kmol m$^{-3}$) |
| $c_p$ | fluid specific heat capacity at constant pressure (J kg$^{-1}$ K$^{-1}$) |
| $D$ | mass diffusion coefficient (m$^2$ s$^{-1}$) |
| $E_{a,k}$ | activation energy for reaction $k$ |
| $g$ | acceleration constant (m s$^{-2}$) |
| $h$ | specific enthalpy (J kg$^{-1}$) |
| $k_1$, $k_2$ | empirical constants in the Forchheimer expression (m$^2$), (m) |
| $k_k$ | specific reaction rate constant of reaction $k$ (s$^{-1}$) |
| $k_k^0$ | collision-frequency factor of reaction $k$ |
| $K_C$ | equilibrium constant |
| $M$ | molecular weight (kg kmol$^{-1}$) |
| $N$ | number of species |
| $N_R$ | number of reactions |
| $P$ | pressure (Pa) |
| $R$ | universal gas constant = 8.314 J mol$^{-1}$ K$^{-1}$ |
| $T$ | temperature (K) |
| $T_{50}$ | methane half-conversion temperature (K) |
| $v$, $v_s$ | velocity, superficial velocity (m s$^{-1}$) |
| $x$ | space co-ordinate (m) |
| $Y$ | mass fraction |

*Greek letters*

| | |
|---|---|
| $\delta$ | distance of the flame front inside the burner thickness from the burnerdeck (m) |
| $\Delta h_{f,i}^0$ | heat of formation for species $i$ (J kg$^{-1}$) |
| $\phi$ | volumetric porosity |
| $\lambda$ | thermal conductivity (W m$^{-1}$ K$^{-1}$) |
| $\lambda_{eff}$ | effective thermal conductivity of the porous medium (W m$^{-1}$ K$^{-1}$) |
| $m$ | dynamic viscosity (kg m$^{-1}$ s$^{-1}$) |
| $\nu'_{k,j}$ | stoichiometric coefficient of the forward reaction $k$ |
| $\nu''_{k,j}$ | stoichiometric coefficient of the backward reaction $k$ |
| $\rho$ | gas density (kg m$^{-3}$) |
| $\omega$ | species source/sink term (kg m$^{-3}$ s$^{-1}$) |

*Subscripts*

| | |
|---|---|
| eff | effective |
| f | formation |
| $i$ | generic species |
| $k$ | reaction |

covered regimes, which is commonly named transition regime.

An important target and challenge for modern natural gas burners for domestic boiler applications is a large power modulation range, capable of satisfying contemporarily a wide variety of users' demands (from hot sanitary water production, requiring on average 25 kW per apartment, down the 2–3 kW required for apartment heating purposes), meanwhile decreasing the number of start-up and switch-off cycles, responsible for high energy loss, significant CO emissions and material stresses due to thermal shock. In this context, notwithstanding the great advantage of the low $NO_x$ emissions over the large modulation range, non-catalytic pre-mixed burners generally suffer from high and almost unacceptable CO and HC emissions at the low $Q$ values (e.g. 200–400 kW m$^{-2}$ corresponding to the lowest power values of the modulation range); the comparatively low flame temperatures occurring in this "weak" radiant regime significantly affect the completeness of methane combustion. Previous studies on FeCrAl alloy metal fibre panels (NIT100S by Acotech, B) [7,8] confirmed that a wide modulation range (10:1) could be achieved with acceptable $NO_x$ emissions (always below 75 ppm), whereas CO and HC concentrations were unacceptably high (exceeding 100 ppmv) below 400 kW m$^{-2}$.

In order to promote complete methane combustion under these operating conditions, the catalytic activation of the burner by depositing a suitable perovskite catalyst ($LaMnO_3$) was conceived and experimentally demonstrated [9]. Over the last 15 years, a number of transition metal-base perovskites have been investigated enlightening high activity towards methane combustion [10–15]. In view of their low cost, if compared to noble metals, and potentially good resistance to sintering and volatilisation, selected perovskites hold some promise for industrial applications in catalytic combustion technologies (catalytic high-temperature combustion, VOC removal, etc.). A weak point of these promising materials, and especially of those formulations that show the prevalent activities towards methane combustion ($LaMnO_3$, $LaCoO_3$, etc.) is their rather low resistance to sulphur [16].

In this contribution, after showing how sulphur poisoning resistance of $LaMnO_3$ can be markedly increased by using MgO as a textural promoter [15], a new catalytic burner (based on the same FeCrAl alloy fibre burner studied in earlier papers [7–9]), catalysed with a $LaMnO_3$ + 17MgO catalyst is presented. The performance of this catalytic burner will be compared to those of the non-catalytic fibre mat and of the simple $LaMnO_3$-catalysed one, showing improvements in terms of durability and CO emissions at low superficial power (power per unit burner surface $Q <$ 600 kW m$^{-2}$).

In a parallel effort, in order to get deep knowledge of the complex mechanisms occurring in porous media combustion and to easily investigate how the catalyst properties can affect the combustion, a preliminary attempt to model combustion in the metal panel has been accomplished by adapting to the present study the code Fastest 3.52, under continuous development at the Institute of Fluid Mechanics in Erlangen University and already applied in the recent past to the modelling of porous foam pre-mixed burners [17].

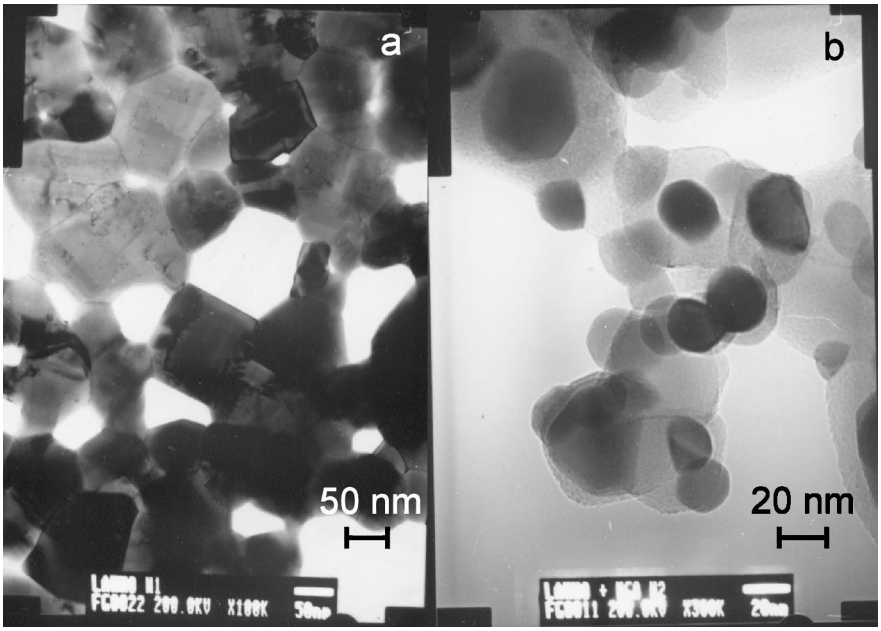


Fig. 1. HRTEM micrographs of $LaMnO_3$ (a) and $LaMnO_3 + 17MgO$ (b) catalysts.

## 2. Experimental

### 2.1. Materials and methods

#### 2.1.1. The catalysts

Perovskite $LaMnO_3$ powders were prepared with and without MgO (perovskite content: 25 wt.%; MgO: balance, corresponding to a 17:1 MgO:$LaMnO_3$ mole ratio), via a modified version of the so-called "citrates method". Solid mixtures of $La(NO_3)_3{\cdot}6H_2O$, $Mn(NO_3)_2{\cdot}6H_2O$ and $Mg(NO_3)_2{\cdot}6H_2O$ (by Fluka) were mixed with a 30 wt.% amount of citric acid and 40 wt.% of water. The obtained solution was slowly heated up to 120°C until a slight gas emission ($NO_x$, CO and water vapour) started. The very viscous liquid generated was then rapidly poured in a stainless steel vessel, kept in oven at 180°C, thereby causing immediate and massive gas formation, which led to the formation of a solid scum, quite friable and porous. The scum was then finely ground in an agate mortar and kept in oven for 4 h in calm air at 900°C.

XRD analyses (Philips PW1710 with Cu Kα radiation monochromator) showed that the typical $ABO_3$ structure was formed in both cases, accompanied by sharp MgO peaks in the promoted catalyst version. HRTEM (JEOL) observations (Fig. 1) allowed to assess the microstructure of the prepared catalysts: the perovskite crystals of the pure $LaMnO_3$ are much larger compared to those of the same perovskite (dark crystals) in the presence of MgO (light crystals); particularly, on the basis of extensive image analysis, the average particle size of the first catalyst was about 100 nm, whereas that of the second ones was just 25 nm. Furthermore, in the promoted catalysts, the perovskite crystals are randomly dispersed among the MgO crystals. On the basis of recent investigations [15], such condition should effectively guarantee improved catalytic activity and a hindering effect on high temperature sintering prolonging the lifetime of the promoted catalyst. Moreover, on the grounds of the studies presented in [16], it is expected as well that the MgO promoter should preferentially react with $SO_2$ arising from the combustion of natural gas odorants or of other sulphur compounds there present.

In order to verify this last hypothesis, portions of the $LaMnO_3$ and of the $LaMnO_3 + 17MgO$ catalyst powders were aged in electric oven at 800°C (a typical operating temperature of the burner in the weak radiant regime) under an air flow with 200 ppmv of $SO_2$. Half conversion temperature measurements were carried out in a temperature programmed combustion quartz reactor according to the operating procedures described in [15] (catalyst load: 0.5 g pelletised by compression, crushing and sieving; catalyst pellet size: 200–400 mm; feed composition: $CH_4 = 2\%$; $O_2 = 18\%$, He = balance; feed flow rate: $1.2\,cm^{-3}\,s^{-1}$; temperature rise rate: $3°C\,min^{-1}$; internal reactor diameter = 4 mm) as a function of the ageing time (up to 30 days).

#### 2.1.2. The FeCrAl alloy fibre burner

The burner mat employed in the present study is the NIT100s FeCrAl alloy panel manufactured by ACOTECH BV (Zwevegem, B). A yarn made of fine metal fibres (rectangular cross section: $10 \times 20\,mm^2$) is knitted to form a textile, approximately 2 mm thick (Fig. 2). The knitted product is a very flexible burner mat, very suitable for applications of complex burner shapes (cylinders, emispheres, cones, etc.).

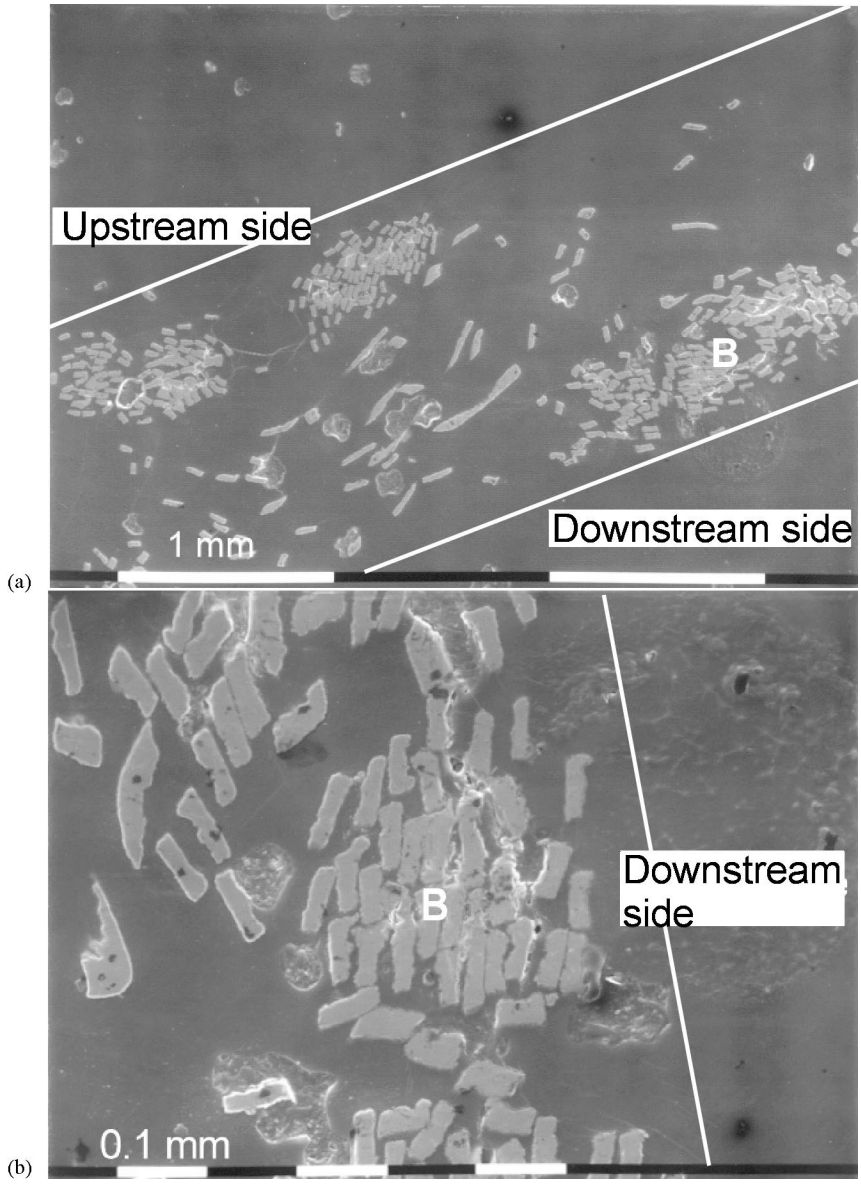


Fig. 2. SEM micrographs of the cross section of the FeCrAl alloy fibre burner NIT100S by ACOTECH BV (Zwevegem, B). (a) Overall view; (b) zoomed view of yarn B.

The fine fibres are made of FeCrAl alloy: chromium = 20.0 wt.%, aluminium = 5.0 wt.%, yttrium = 0.10 wt.%, silicon = 0.30 wt.%, manganese = 0.08 wt.%, copper = 0.03 wt.%, carbon = 0.03 wt.%, iron = balance. This refractory steel is well-known for its outstanding oxidation resistance at temperature up to 1200°C.

The surface area of the flat burners was 160 mm × 250 mm.

Thermo-physical data of the mat, useful for model calculation (Section 3) were provided directly by the manufacturer or found in the literature. The volumetric porosity of the mat is about 85%. Because of the open structure, at 30% $E_a$, the pressure drop across the material is extremely low: from 0.4 mm of water column at 500 kW mm$^{-2}$ to 3 mm of water column at 5000 kW m$^{-2}$. As concerns the thermal conductivity, some data relating to a sintered FeCrAl alloy fibre panel are available [18]: 0.15 W m$^{-1}$ K$^{-1}$, across the thickness, 0.88 perpendicularly (parallely to the panel surface). The material emissivity, a very important parameter because it influences the surface temperature and the radiation efficiency, was experimentally determined by the manufacturer: it increases with the power density, from 0.72 at 200 kW m$^{-2}$ to 0.76 at 800 kW m$^{-2}$.

The FeCrAl alloy panels owes its outstanding high-temperature oxidation resistance to the formation of an $\alpha$-$Al_2O_3$ oxide protecting layer, which in the present case is also quite useful for catalyst anchoring purposes. The formation of such layer normally occurs during operation for non-catalytic burners, whereas it has to be promoted

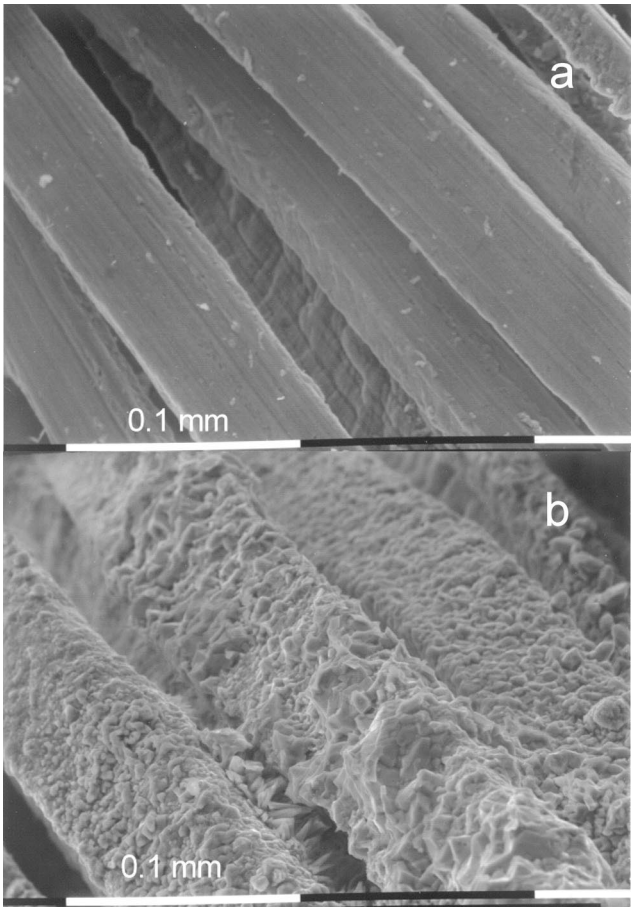


Fig. 3. Close SEM views of virgin (a) and pre-oxidised (b) FeCrAl alloy fibres.

by a suitable high-temperature treatment under oxidising atmospheres prior to catalyst deposition. All the burners were thus calcined at 900°C for 4 h. In such conditions, the aluminium present in the alloy migrates from the core of the fibres to their surface and forms an uniform coating of $\alpha$-$Al_2O_3$ (Fig. 3), whose function is just that to protect the core of the fibres from further oxidation. The presence of yttrium helps in strengthening the bond between the $\alpha$-$Al_2O_3$ layer and the basic alloy [19].

*2.1.3. The catalytic burners*

Taken into account that combustion should in part take place only in a rather thin region near the outlet surface, two panels were deposited respectively with the $LaMnO_3$ and $LaMnO_3 + 17MgO$ phases just at that location. The deposition technique adopted was a simple and cheap route, based on spray-pyrolysis, previously developed and optimised [15]. Two different solutions were prepared by mixing the appropriate precursor salts among $La(NO_3)_3{\cdot}6H_2O$, $Mn(NO_3)_3{\cdot}6H_2O$ and, when needed, $Mg(NO_3)_2{\cdot}6H_2O$, dosed in stoichiometric ratio to a 30 wt.% amount of citric acid and diluted in water. The resulting equivalent $LaMnO_3$ concentration was about 0.2 mol $l^{-1}$. The solutions were then sprayed over the downstream surface of the panels, just taken out of an electric oven where pre-heating at high temperature (about 900°C) had been carried out. Due to the in situ pyrolysis occurring on the hot panel surface, catalyst crystallisation occurred leading to a fairly uniform load of catalyst (Fig. 4a), rather well anchored to the alumina phase despite some catalyst detachment was observed occasionally (Fig. 4b). Repeated cycles allowed to deposit about 0.075 kg $m^{-2}$ of the perovskite phases (about 3 g of catalyst over each burner).

Previous studies enlightened how the perovskite may undergo partial deactivation due to interaction with the $\alpha$-$Al_2O_3$ fibre coating, leading to lanthanum aluminates formation [8]. The adopted deposition technique, based on a repeated procedure (a number of cycles that enables the deposition of a desired catalyst amount over the firing surface), leads to a multi-layer catalyst structure. If the catalyst fraction immediately close to the alumina suffers from deactivation, the covering catalyst layers result almost unaffected.

In order to further stabilise and have a complete crystallisation of the catalysts, the burners were finally calcined at 900°C for 4 h in calm air.

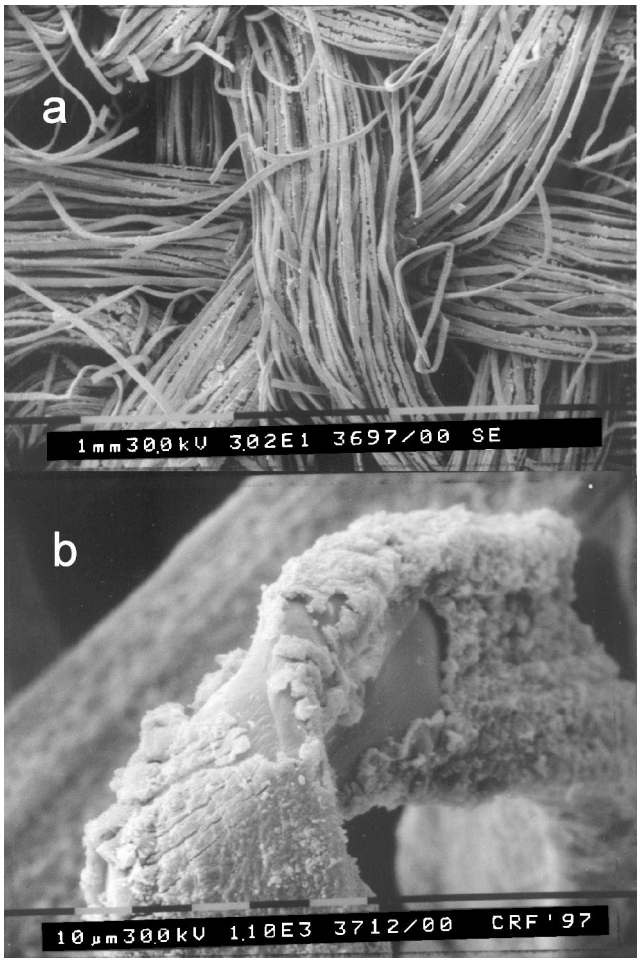


Fig. 4. SEM observations of the $LaMnO_3$-catalysed fibre burner. (a) Overall view of the fibre texture; (b) zoomed view of a catalysed fibre showing some catalyst detachment areas.

*2.1.4. Sulphur ageing of the catalytic burners*

The two catalytic panels, after having evaluated their performance in the test rig (see next section), were submitted to ageing in an electric oven for 36 h at 800°C under a 100 ml $min^{-1}$ air flow containing 200 ppmv of $SO_2$. Such a concentration was conservatively chosen several times higher than that usually added to commercial natural gas as odorant (about 8 ppmv in Italy as THT) so as to accelerate the poisoning effect. The two catalytic panels, based on the $LaMnO_3$ and $LaMnO_3 + 17MgO$ catalysts, were then tested again in the pilot plant described below in order to enlighten any effect of the sulphur poisoning over their performance.

*2.1.5. Pilot plant testing of the pre-mixed burners*

The two catalytic burners and the non-catalytic one (reference) were tested in a specific pilot plant (maximum power: 40 kW). The boiler configuration for flat burners is represented in Fig. 5. Air and methane are pre-mixed in a Venturi; the mass flow rates are electronically controlled by a blower (for the air) and a modulating electro-valve (for the methane from the net). In the plenum chamber, two plates are sequentially placed: the lower, a solid plate, to divert the flow towards the peripheral part of the chamber and the upper, a perforated plate, to balance the pressure of gas mixture under the burner, in order to achieve a correct distribution of the feed gas flow over the burner. The burner at the basis of the combustion chamber is fitted horizontally and fires upwards. In the wall of the combustion chamber, four quartz windows are mounted for internal inspection and to observe the burner firing surface. A quartz tube could be inserted in the combustion chamber for gas sampling purposes at different locations (S1, S2 and S3 in Fig. 5b) and at different heights over the burner surface. Just above the combustion chamber, the flue gases were cooled through a "finned-tube" type heat exchanger and dispersed through a chimney.

Tests were carried out in the power input range 200–800 kW $m^{-2}$ at different excess-air values: 5–90%. The composition of the exhaust gas was analysed through a set of continuous analysers by Elsag–Bailey: a $NO_x$ chemiluminescence analyser, a FTIR analyser for CO and $CO_2$, an $O_2$ paramagnetic detector. The composition of the flue gas ($CO_2$, CO, $NO_x$) is expressed as ppmv and referred to dry gases at 0°C and 1013 mbar. The upper and lower surface temperatures were recorded for each test at the S2 location through specific thermocouples.

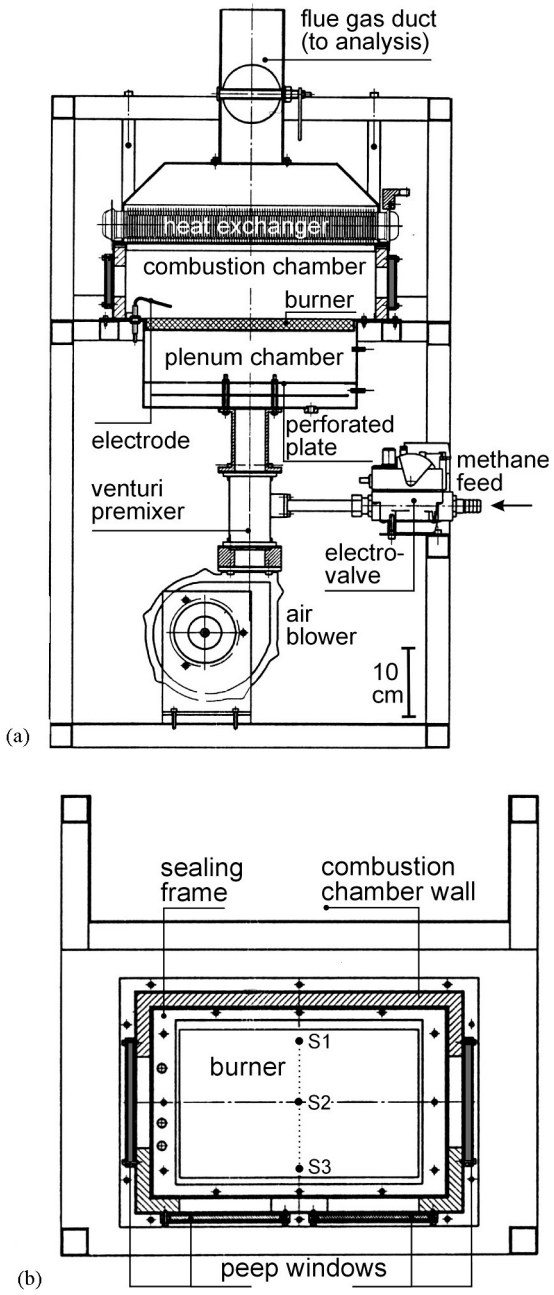


Fig. 5. Cross sections of the pilot boiler for the assessment of the pre-mixed burner performance (courtesy of Ikerlan, Victoria, ES). (a) Front view; (b) upper view of the burner showing the S1, S2 and S3 flue gas sampling locations.

*2.2. Results and discussion*

The data in Fig. 6, obtained with catalysts powders, just confirm the increased activity and sulphur-poisoning resistance of the $LaMnO_3 + 17MgO$ catalyst over the simple $LaMnO_3$ one. In fresh state, the half conversion temperature of the MgO promoted catalyst (485°C) is about 50°C lower than that of its non-promoted counterpart. This would be a consequence of the small crystal size of the perovskite crystals in the $LaMnO_3 + 17MgO$ catalyst, which should expose a larger catalytic surface area than that of the bulk perovskite crystals of the $LaMnO_3$ catalyst (see Fig. 1), despite the presence of just one-fourth of pervoskite mass. Moreover, some direct contribution of the MgO promoter to methane conversion cannot be excluded [15].

The gap between the catalytic activity of the two catalysts is increased under aged conditions: if the $LaMnO_3$ promoted catalyst gets rapidly deactivated ($T_{50}$), the MgO promoted perovskite faces a much lower rate of poisoning, especially after the first day of poisoning treatment and only

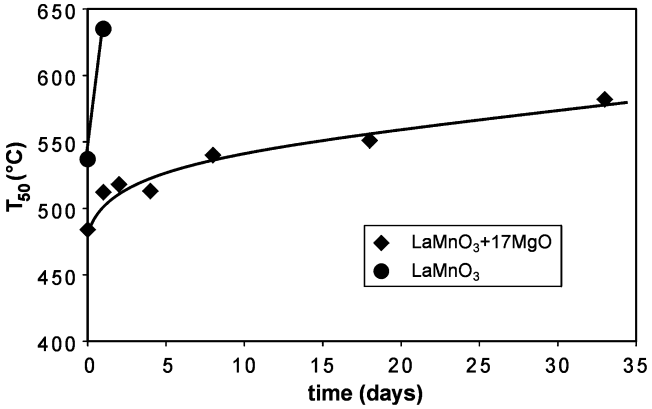


Fig. 6. Effect of prolonged ageing under $SO_2$-laden atmosphere on the catalytic activity (half conversion temperature) of $LaMnO_3$ and $LaMnO_3 + 17MgO$ catalyst powders.

after 30 days it gets to a half-conversion temperature just 50°C lower than that reached by its counterpart after 1 day ageing. These results were the spur to develop the catalytic fibre metal burner based on the MgO-promoted catalyst, whose performance will be discussed in the following. XRD analysis of the 30-days-aged $LaMnO_3 + 17MgO$ catalyst confirmed the presence of significant amounts of $MgSO_4$, whose preferential formation prevented rapid perovskite poisoning. It is obviously expected that a longer exposition of the $LaMnO_3 + 17MgO$ catalyst to the $SO_2$-laden stream, once that most MgO promoter is involved in the sulphates formation, will progressively cause $LaMnO_3$ poisoning.

Fig. 7 provides a comparison of the combustion regimes (radiant, transition and blue-flame) of the three pre-mixed burners tested (non-catalytic, $LaMnO_3$-catalysed, $LaMnO_3 + 17MgO$-catalysed) in the $Q$–$E_a$ dominion. For each panel, the lines limiting the various combustion

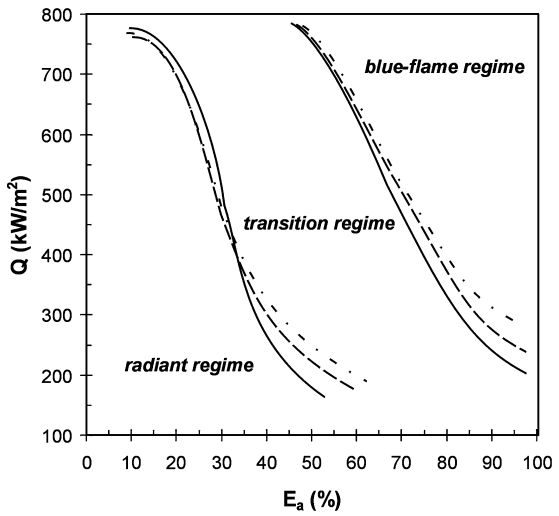


Fig. 7. Combustion regime map in the $Q$–$E_a$ dominion for the non-catalytic (—), the $LaMnO_3$ (– – –) and the $LaMnO_3 + 17MgO$ (-·-·-) catalytic burners.

regimes are drawn. As mentioned earlier, $E_a$ being constant, the blue-flame regime prevails at high $Q$ values while the radiant one at low $Q$ values.

Fig. 7 shows how the differences in the behaviour of the three burners are not remarkable. On the grounds of their catalytic activity, that helps to keep part of the combustion inside the burner, the catalytic fibre mats reduce the area of the blue flame zone and expand the radiant regime region for $Q$ values lower than about 400 kW m$^{-2}$. The effect is more evident for the panel catalysed with the MgO-promoted catalyst, a likely consequence of its prevalent higher catalytic activity. The slight contraction of the radiating combustion area for both the catalytic panels, compared with the non-catalytic one at $Q > 400$ kW m$^{-2}$, can perhaps be explained by the fact that at the high panel temperatures, typical of these specific power inputs, the combination of gas thermal expansion and decreased permeability (due to the presence of the catalyst in the porous burner texture) implies a strong acceleration of the flue gases inside the porous matrix that limits the effect of the catalyst activity in pre-igniting the combustion and keeping it inside the burner (see Section 3.4 for more details).

As concerns CO and $NO_x$ emissions of the fresh burners as a function of the excess air and for selected $Q$ values (Figs. 8 and 9, respectively), the following conclusions can be drawn:

1. $NO_x$ emissions are almost unaffected by the presence of the catalysts at any operating conditions. This was also observed in earlier investigations [8,9]. The $NO_x$ level of the burner remains good over the entire range of operating conditions with an expected slight increase with the $Q$ value (higher flame temperatures).
2. CO emissions are strongly reduced at low $Q$ values (<380 kW m$^{-2}$) and for excesses of air lower than 15% by the presence of the catalyst. This should help in achieving reliably the 10:1 power modulation range (the major objective of the present burner development as declared in Section 1), provided thermal and sulphur resistance of the catalysts proves to be satisfactory.

The CO concentration data plotted in Fig. 10, concerning the flue gases sampled at different distances from the burnerdeck at the S1, S2 and S3 locations over the non-catalytic and the $LaMnO_3$-catalysed burner, elucidate where most of the CO emissions are generated. Close to the burner perimeter (S1 and S3 locations) there are the highest CO emissions. The most likely explanation of that should lie in a localised cooling effect of the sealing system that locally quenches the reaction and hampers the achievement of combustion completeness. However, it is quite satisfactory to notice how, especially at those locations, the effect of the catalyst in lowering the CO emissions is particularly remarkable. As later on detailed 2D and 3D model simulations are planned to further elucidate this point.

Shifting finally to analysing the performance of the $SO_2$-aged versus fresh catalytic burner performances in

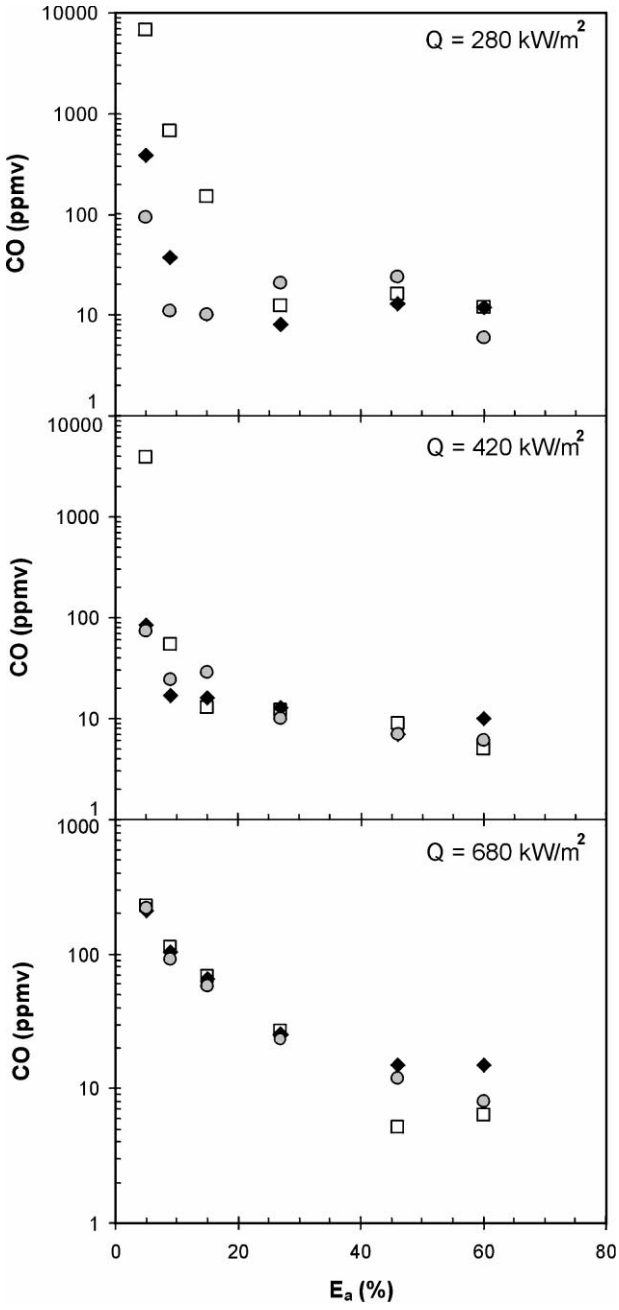


Fig. 8. CO emissions (0°C, 1013 mbar, dry gases) of the non-catalytic (□), the $LaMnO_3$ (◆) and the $LaMnO_3 + 17MgO$ (◉) catalytic burners as a function of $E_a$ and for three different $Q$ values.

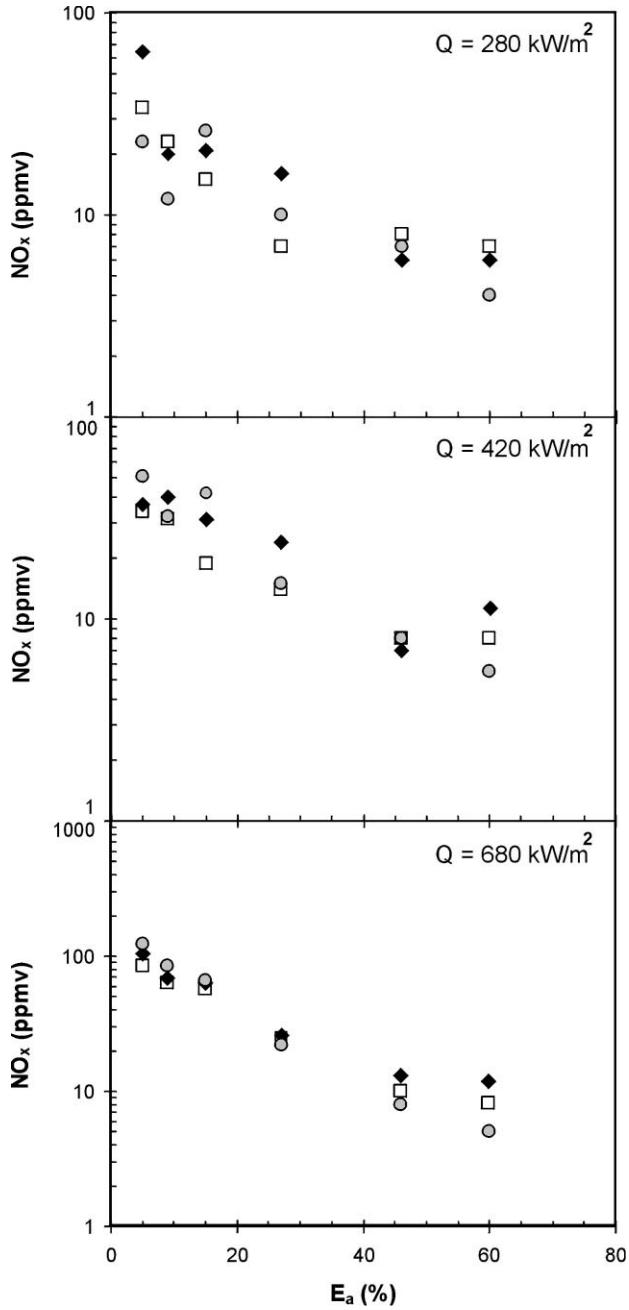


Fig. 9. $NO_x$ emissions (0°C, 1013 mbar, dry gases) of the non-catalytic (□), the $LaMnO_3$ (◆) and the $LaMnO_3 + 17MgO$ (◉) catalytic burners as a function of $E_a$ and for three different $Q$ values.

terms of CO (Fig. 11) and $NO_x$ (Fig. 12) emissions, the following considerations can be drawn:

1. $NO_x$ emissions are once again almost unaffected by the sulphur ageing of the catalyst, if not even slightly improved (Fig. 12b).
2. Conversely, as expected, CO emissions are severely increased by the sulphur-poisoning treatment for the $LaMnO_3$-catalysed burner, despite they still remain lower than those of the non-catalytic burner (not reported in Fig. 11 for the sake of clarity).
3. The CO emissions of the fibre burner catalysed with MgO-promoted lanthanum manganate are not worsened by the ageing treatment, if not even improved (at certain operating conditions).

These results strongly indicate that the $LaMnO_3 + 17MgO$ catalytic burner should possess the required activity and durability in the presence of sulphur compounds.

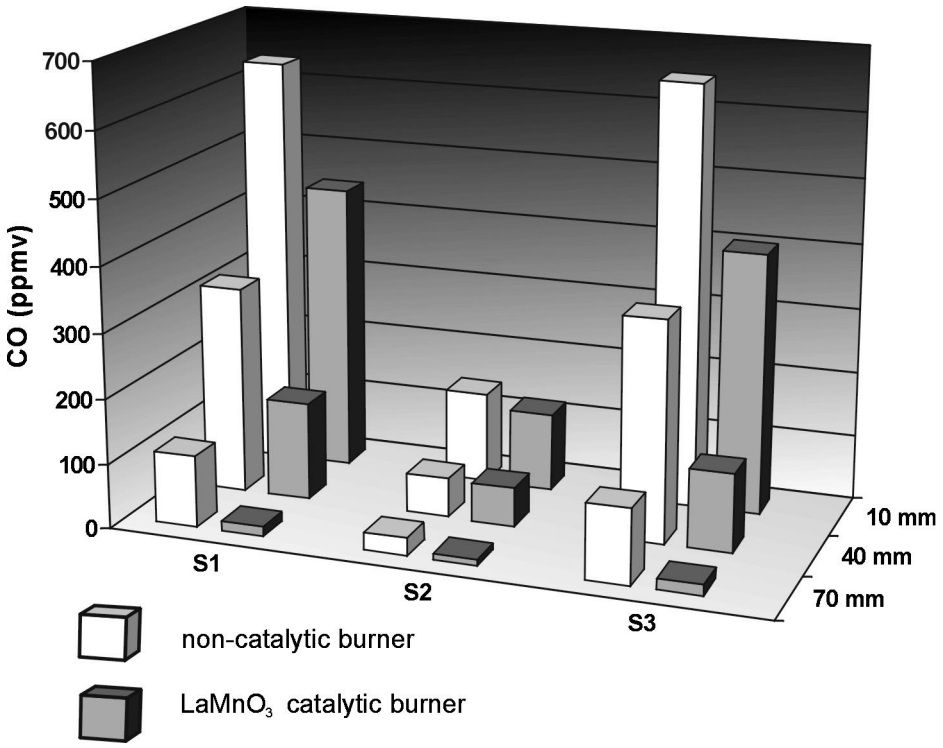


Fig. 10. CO concentration at the S1, S2 and S3 flue gas sampling locations as a function of the distance from the downstream surface of the non-catalytic and the $LaMnO_3$ catalytic burner ($Q = 290\,kW\,m^{-2}$; $E_a = 10\%$).

## 3. Preliminary modelling investigation

As mentioned above, a model has been assembled considering differential mass, momentum and heat balance equations in the plenum chamber, in the porous medium and in the combustion chamber. These equations are listed in the following sections.

### 3.1. Governing equations in the gas phase

The reacting gaseous mixture in the plenum and in the combustion chamber was modelled by considering the set of governing equations, valid for a laminar flow in non-isothermal and in steady-state conditions. In the following, the differential equations for the conservation of mass, momentum and energy are written in vectorial notation:

$$\nabla(\rho v) = 0 \quad \text{(continuity equation)} \tag{1}$$

$$\nabla\,(\rho v Y_i - \rho D_i \nabla Y_i) = \omega_i \quad \text{(species conservation equation)} \tag{2}$$

$$\nabla(\rho v v - \mu \nabla v) = -\nabla P - \nabla(\mu \nabla v) + \rho g \quad \text{(momentum equation)} \tag{3}$$

$$\nabla(\rho v c_p T - \lambda \nabla T) = \sum_{i=1}^{N} \omega_i \Delta h^0_{f,i} + \nabla\left(\sum_{i=1}^{N} \rho h_i D_i \nabla Y_i\right) \quad \text{(energy equation)} \tag{4}$$

The skeletal mechanism for lean methane–air combustion [20], consisting of 84 reversible reactions among 19 reacting species plus nitrogen, is used to compute the combustion chemistry in the flame. Nitrogen chemistry was not computed, taking into account that its influence on heat and mass balances is almost negligible, while computation time would be seriously affected. Eq. (2) was only solved for $N-1$ species. The mass fraction $Y_N$ of the $N$th species, the nitrogen $N_2$, was obtained from the algebraic relationship

$$Y_N = 1 - \sum_{i=1}^{N-1} Y_i \tag{5}$$

The density $\rho$ was calculated for a mixture of perfect gases on the basis of the ideal-gas law. The viscosity $\mu$ and the heat conductivity $\lambda$ of the mixture and the mass diffusion coefficient $D_i$ of each species $i$ present in the mixture were calculated on the basis of the pure species properties using semi-empirical approximations [21–23]; the pure species properties were estimated from kinetics gas theory [24]. The specific heat capacity $c_p$ of the mixture as well as all other thermodynamics data were obtained from the CHEMKIN II data base [25]. The rate of formation and destruction of species $i$ due to chemical reactions enters as a source term $\omega_i$ into the species transport equations

$$\omega_i = M_i \sum_{k=1}^{N_R} (\nu''_{i,k} - \nu'_{i,k}) k_k \left( \prod_{\text{reactants}} c_i^{\nu'_{i,k}} - \frac{1}{K_C} \prod_{\text{products}} c_i^{\nu''_{i,k}} \right) \tag{6}$$

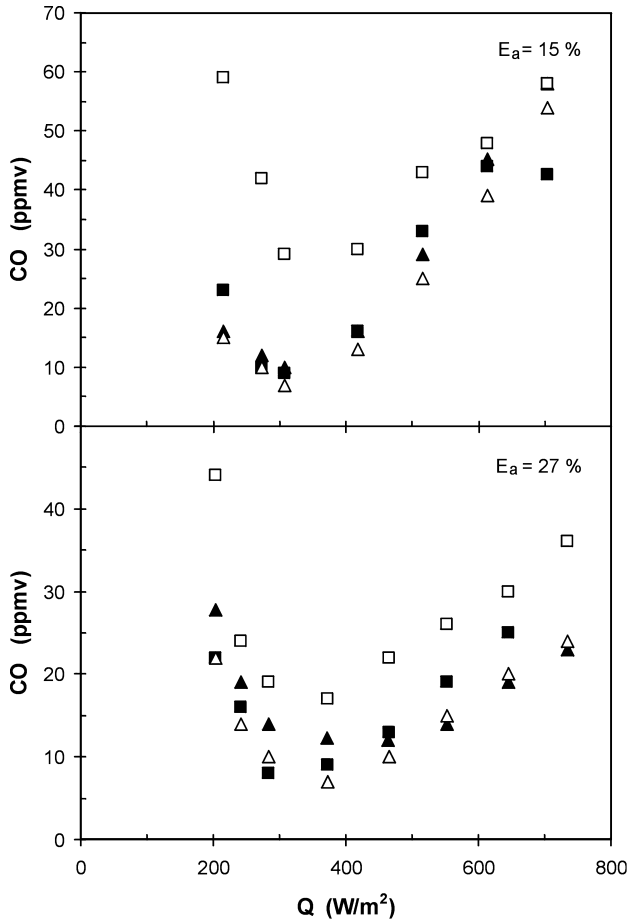


Fig. 11. Effect of $SO_2$ poisoning on the CO emissions of the two catalytic burners tested as a function of $Q$ for two $E_a$ values. (■, □): $LaMnO_3$ catalytic burner; (▲, △): $LaMnO_3$+17MgO catalytic burner. Full symbols: fresh catalysts; empty symbols: aged catalysts.

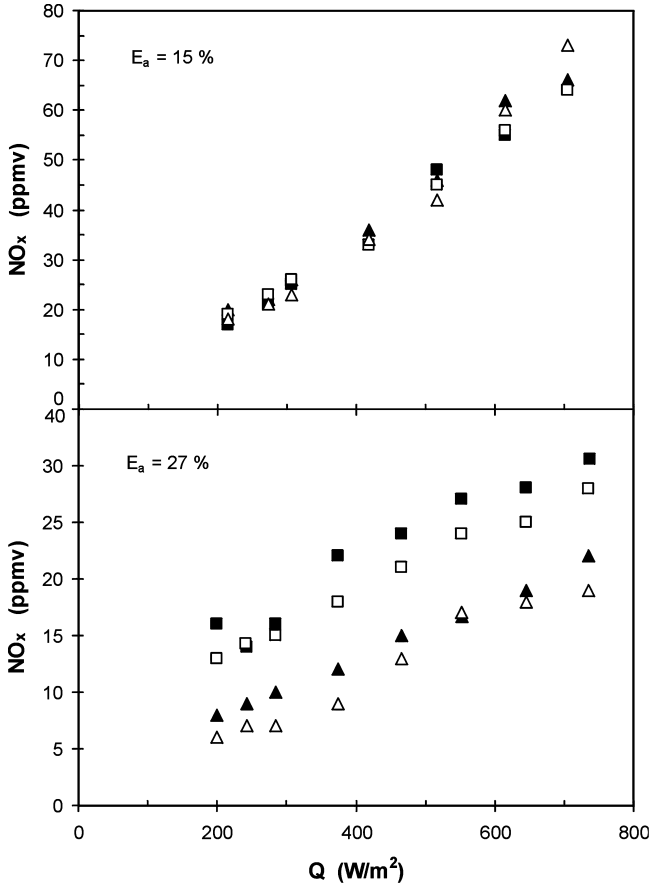


Fig. 12. Effect of $SO_2$ poisoning on the $NO_x$ emissions of the two catalytic burners tested as a function of $Q$ for two $E_a$ values. (■, □): $LaMnO_3$ catalytic burner; (▲, △): $LaMnO_3 + 17MgO$ catalytic burner. Full symbols: fresh catalysts; empty symbols: aged catalysts.

where $N_R$ is the number of reactions and $\nu'_{i,k}$ $\nu''_{i,k}$, are the stoichiometric coefficients of the reactants $A_i$ and products $B_i$, respectively, in the generic reaction $k$

$$\sum_{i=1}^{N-1} \nu'_{i,k} A_i \Leftrightarrow \sum_{i=1}^{N-1} \nu''_{i,k} B_i \tag{7}$$

The reaction velocity coefficient $k_k$ is determined on the basis of the modified Arrhenius expression

$$k_k = k_k^0 T^{\beta_k} \exp\left(-\frac{E_{a,k}}{RT}\right) \tag{8}$$

The collision parameter $k_k^0$, the temperature exponent $\beta_k$ and the activation energy $E_{a,k}$ were specified for each reaction on the basis of the indications provided in [20]. The reverse reaction rates are determined from the Gibbs-free enthalpy using basic thermodynamic principles [25]. The last term of the right-hand side of Eq. (4) is an additional energy-flux term, caused by interdiffusion processes, in binary and multi-component systems [26].

### 3.2. Governing equations in the porous medium

As a first approximation, the solid matrix was considered as inert and not influencing the reactions within the porous medium, but strongly affecting the gas flow and heat transfer. As a consequence, the reaction kinetics of all reactions in the gas phase inside the porous medium were kept equal to those previously indicated in [20].

According to a simplified approach, a local thermal equilibrium between the solid and the gas phase was assumed (pseudo-homogeneity); this assumption is acceptable when the heat transfer coefficient and transfer area between the fluid phase and the solid matrix are large [27]. In modelling heat transfer inside the porous medium, radiation represents the most difficult component to take into account due to the integral-differential expression that governs the radiation flux equation for an absorbing, emitting and scattering medium. In the field of combustion into porous media, several different approximations can be considered so as to simplify the radiation problem [28]. Due to its simplicity at the cost of sacrificing some accuracy the radiant flux within the metal panel was approximated with the Rosseland

diffusion equation [29], acceptable as far as the solid can be considered as optically dense [30]. The porous medium is thus modelled as a pseudo-homogeneous system based on volume-averaged properties such as the effective thermal conductivity [29], which consists of all the major heat transfer mechanisms: convection, conduction, radiation.

Only in the porous medium region, under all these assumptions, the governing equations of mass, momentum, and heat transfer were suitably modified, by introducing the superficial velocity $v_s$, the porosity $\phi$, the thermal effective conductivity $\lambda_{eff}$, and by adopting the Darcy–Forchheimer formulation linking pressure drop to $v_s$ instead of the momentum transport equation

$$\nabla(\rho v_s) = 0 \quad \text{(continuity equation)} \tag{9}$$

$$\nabla(\rho v_s Y_i - \rho\phi D_i \nabla Y_i) = \phi\omega_i \quad \text{(species conservation equation)} \tag{10}$$

$$\nabla P = -\frac{\mu}{k_1} v_s - \frac{\rho}{k_2}|v_s| v_s \quad \text{(Darcy–Forchheimer equation)} \tag{11}$$

$$\nabla(\rho v_s c_p T - \lambda_{eff}\nabla T) = \phi\sum_{i=1}^{N}\omega_i \Delta h^0_{f,i} + \nabla\left(\sum_{i=1}^{N}\rho h_i \phi D_i \nabla Y_i\right) \quad \text{(energy equation)} \tag{12}$$

### 3.3. Boundary conditions

The model was solved over a single dimension (across the axial co-ordinate, that is perpendicular to the burner surface) over a domain of the numerical computation runs from $x = -6.2$ to 70 mm. It consists of three regions: a part of the plenum chamber, the metal panel and a part of the combustion chamber. The following boundary conditions over the entire domain were applied:

1. At the inlet, the axial velocity, the temperature and the species concentrations were pre-determined.
2. At each burner interfaces, continuity of the gradients and the values for all the variables was imposed. At the exit surface of the porous medium, it was additionally taken into account that heat is radiated directly from the surface to the heat sink, by the integral relationship valid for a black body (by considering the material emissivity, the local temperature, the heat sink geometry and temperature, etc.).
3. At the outlet boundary, all gradients were set to zero.

### 3.4. Model calculations

Eqs. (9)–(12) can be formulated in a general elliptical transport equation type

$$\nabla(\rho v\Phi - \Gamma_\Phi \Delta\Phi) = S_\Phi \tag{13}$$

where $\Phi$ is the transported variable, $\Gamma_\Phi$ the corresponding diffusion coefficient and $S_\Phi$ represents source and sink of $\Phi$. For the spatial discretisation of Eq. (13), a finite volume method was employed. The solution domain was discretised over a grid mesh. Typical grid spacing was 0.05–1 mm, depending on the local variable gradients: the higher the gradients, the lower the grid spacing required to achieve conversion and to limit calculation errors. The diffusive fluxes were discretised using a central differencing scheme, whereas the contribution of the convective transport was evaluated using a deferred correction scheme [31]. The solution of the resulting system of algebraic equations was obtained through a semi-implicit procedure [32], while the coupling of pressure and velocity was accomplished via the SIMPLE algorithm [33].

A first clear indication of the preliminary calculations carried out with the proposed model was the impossibility to achieve flame stabilisation over the burnerdeck unless unrealistically low values of the axial heat conductivity of the burner were considered. Flashback conditions were always generated by modelling calculations whenever the burnerdeck temperature reached values higher than about 800°C. In line with the conclusions of the recent work of Bouma [34] on the modelling of pre-mixed porous foam burners, this occurrence has to be attributed primarily to the pseudo-homogeneous nature of the model. As clearly demonstrated by Bouma, when the combustion is ignited in the gas phase inside a burner pore, the gas temperature might locally exceed the solid temperature by hundreds of degrees, depending on the $Q$ and $E_a$ values. In this context, the solid matrix provides a quenching effect that favours flame stabilisation. Some role in flashback prevention might be played by radical termination reactions over the pore walls, too.

Under these circumstances, in order to simulate the combustion conditions experimentally observed over the burner, the following decisions were made:

1. The combustion mechanism [20] was kept valid only in a limited region of a given thickness ($\delta$) inside the burner, close to the burnerdeck.
2. In the other portions of the burner, all kinetics constants were set equal to zero.

The thickness of such region ($\delta$) can be used as the only fitting parameter of the model.

Due to the current impossibility to implement a proper catalytic reaction set, it was strongly imposed the occurrence of no modification at the kinetic level in the tentative modelling of the catalytic burner. On the other hand, the catalyst should ignite combustion at lower temperatures, anticipating the spatial location of the flame front inside the porous medium. For this reason, the fitting parameter $\delta$ can, to some extent, account for the effect of catalytic reactions in the present model.

The results of model calculations for the non-catalytic and the $LaMnO_3$-catalysed burner (fresh state) against the experimental CO concentration and temperature values,

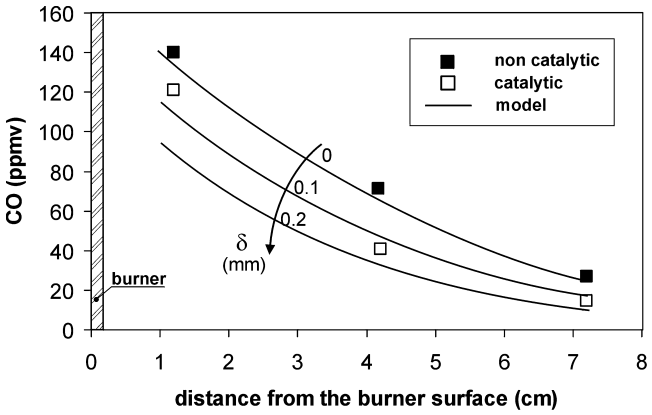


Fig. 13. Measured CO concentrations in the flue gases leaving the non-catalytic (■) and the $LaMnO_3$ catalytic (□) burners at the S2 location at $Q = 298\,kW\,m^{-2}$ and $E_a = 9.8\%$. Model predictions for different penetrations of the flame front inside the burner matrix are also reported for comparison purposes.

obtained for given $Q$ and $E_a$ values at the S2 sampling location, are shown in Fig. 13 as a function of $\delta$. Similar results are obtained for all $Q$ and $E_a$ values in the radiant regime operating mode.

The non-catalytic CO emission is rather well represented by a burner condition of $\delta = 0$. Despite no reaction takes place inside the burner, back radiation from the combustion front, starting immediately downstream the burner, still keeps the burner temperature quite high (see Fig. 14), thereby enabling a fully radiating regime. Similar results were obtained by Nakamura et al. [35] in modelling the surface combustion of methane over a pre-mixed porous alumina burner; good fitting of the experimental data was obtained by assuming that combustion took place almost exclusively inside the combustion chamber and was strongly inhibited in the porous medium.

Conversely, the catalytic panel behaviour is better predicted by allowing a $\delta$ value of about 0.1 mm. This is not surprising at all, since catalyst-supported combustion reaction schemes (e.g. enhanced radical formation) should actually help to pre-ignite the combustion somewhat inside the burner.

A close view of the concentration profiles of $CH_4$, CO and $CO_2$ across the burnerdeck is provided in Fig. 14. Such profiles are quite in-line with those typically encountered with the GRI-mech reaction scheme in plug-flow reactors [20,34]. Lower CO emissions are originated in the flame front when part of methane combustion takes place inside the burner. As a consequence, lower CO concentrations are kept along the entire combustion chamber, where a severe further abatement of CO is in any case achieved (Fig. 13).

Simulated temperature profiles are also plotted in Fig. 14 and compared to the experimental values measured by thermocouples touching the inlet and outlet burner surfaces. The agreement between predicted and measured temperature values is only fair, but the reliability of the thermocouple measurements is questionable for at least two reasons:

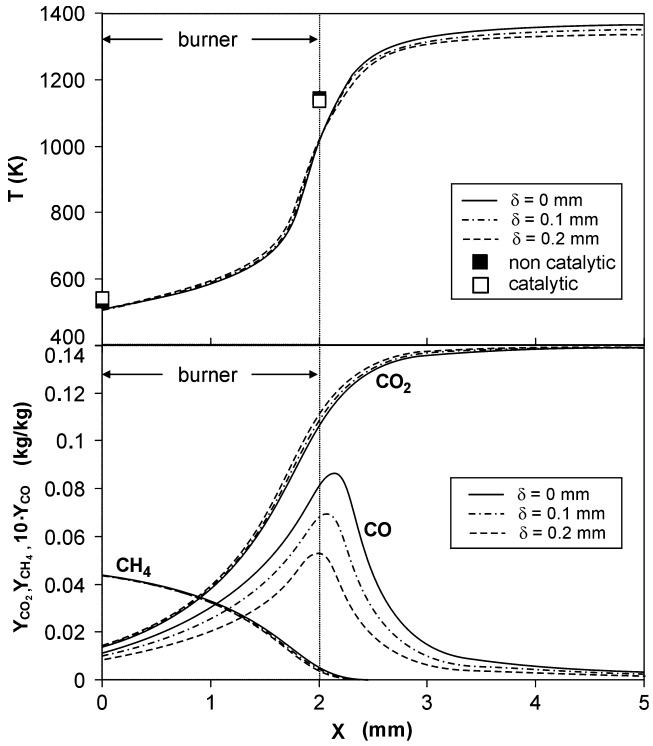


Fig. 14. Calculated temperature and concentration profiles across the burner along the $x$ co-ordinate and for different $\delta$ values (same operating conditions as Fig. 13). Temperature values measured at the S2 location for the non-catalytic and the $LaMnO_3$ catalytic burners are indicated, as well.

1. The burner matrix is rather heterogeneous (Figs. 2 and 4).
2. The temperature of the thermocouple tip (size: 0.5 mm) should be influenced not only by the touched solid fibres, but also by the surrounding gaseous environment, which, according to model simulations, should undergo a rapid heating owing to the combustion process.

If this last issue were true, as likely, the measured temperature values should be representative of the entire combustion region and not only of the burner surface. From this standpoint, the model performance could actually be considered as satisfactory.

Despite a more fundamentally sound two-phase model approach is required [34], it can be concluded that the simple model developed can actually predict the local performance of the non-catalytic burner and, by the use of a single fitting parameter ($\delta$), also that of its catalytic counterpart. Work is in progress to extend the model to 2D and 3D geometries so as to properly predict the localised CO emissions, likely generated at the burner sealing perimeter by some cooling effects (Fig. 10).

## 4. Conclusions

On the basis of the presented results, it can be concluded that the development of a catalytic burner based on FeCrAl

alloy fibre mats (NIT100s by ACOTECH) deposited with the MgO-promoted $LaMnO_3$ was a success and a step forward towards practical application of this type of catalytic burner in high-modulation domestic boilers based on pre-mix burners. Compared to formerly developed catalytic fibre burners based on the non-promoted $LaMnO_3$ catalyst [8,9], lower CO emissions at $Q$ values of about 200–400 $kW\,m^{-2}$ were achieved, especially after ageing under $SO_2$ atmospheres, owing to the effect of the promoter (MgO tends to selectively react with $SO_2$ to form $MgSO_4$, thereby preventing poisoning of the perovskite catalyst). Long-term tests are now planned on the new catalytic burner in order to fully assess its durability under practical operating conditions.

A more fundamental insight in the complex combination of heat, mass and momentum transfer mechanisms governing the performance of the catalytic burner could be gained through a comprehensive numerical model. A first step towards such a model was taken by elaborating a mono-dimensional model lumping the heterogeneous nature of the porous burner into a pseudo-homogeneous approach. This allowed to achieve rather good fitting of the experimental data for both catalytic and non-catalytic burners by means of a single fitting parameter (i.e. the starting position of the flame front inside the burner). Further developments are though needed in order to properly predict the conditions in which the flame is established at or below the burnerdeck or those in which flash-back actually takes place. A new two-phase model is being developed on purpose to tentatively include reaction schemes involving catalytically promoted steps as well as radical termination reactions over the burner pore walls. This model will then have to be extended to 2D and 3D in order to properly evaluate localised CO generation at the burner sealing locations. Only at that stage, the model will be ready for accurate design purposes.

## References


[1] K.J.A. Hargreaves, H.R.N. Jones, D.B. Smith, Developments in burner technology and combustion science, in: Proceedings of the 52nd Institution of Gas Engineers Autumn Meeting, Communication no. 1309, London, 12 November 1986, pp. 1–31.

[2] J.D. Sullivan, Basic Research on Radiant Burners, Alzeta Corporation, Report no. 91-7027-167, Santa Clara, CA, 1991.

[3] R. Viskanta, Interaction of combustion and heat transfer in porous inert media, in: Proceedings of the Eighth International Symposium on Transport Phenomena in Combustion, San Francisco, USA, 1995.

[4] S.B. Sathe, R.E. Peck, T.W. Tong, A numerical analysis of heat transfer and combustion in porous radiant burners, Int. J. Heat Mass Transfer 33 (1990) 1331–1338.

[5] S.B. Sathe, R.E. Peck, T.W. Tong, Flame stabilization in inert porous media: a numerical study, Comb. Sci. Technol. 70 (1990) 93–109.

[6] P. Hsu, R.D. Matthews, The necessity of using detailed kinetics in models for pre-mixed combustion within porous media, Comb. Flames 93 (1993) 457–466.

[7] G. Saracco, S. Sicardi, V. Specchia, R. Accornero, M. Guiducci, M. Tartaglino, On the potential of fibre burners to domestic burners applications. An experimental study, Gaswärme Int. 45 (1996) 24–31.

[8] G. Saracco, I. Cerri, V. Specchia, R. Accornero, Catalytic pre-mixed fibres burners, Chem. Eng. Sci. 54 (1999) 3599–3608.

[9] I. Cerri, G. Saracco, F. Geobaldo, V. Specchia, Development of a methane pre-mixed catalytic burner for domestic applications, Ind. Eng. Chem. Res. 39 (2000) 24–33.

[10] H. Arai, T. Yamada, K. Educhi, T. Seiyama, Catalytic combustion of methane over various perovskite-type oxides, Appl. Catal. A: Gen. 26 (1996) 265–273.

[11] J.G. McCarty, H. Wise, Perovskite catalysts for methane, combustion, Catal. Today 8 (1990) 231–240.

[12] T. Seiyama, in: L.G. Tejuca, J.L.G. Fierro (Eds.), Properties and Applications of Perovskites-Type Oxides, Vol. 50, Dekker, New York, 1993 (Chapter 10) pp. 215–234.

[13] D. Klvana, J. Vaillancourt, J. Kirchnerova, J. Chaouki, Combustion of methane over $La_{0.66}Sr_{0.34}Ni_{0.3}Co_{0.7}O_3$ and $La_{0.6}Sr_{0.4}Fe_{0.4}Co_{0.6}O_3$ prepared by freeze-drying, Appl. Catal. A: Gen. 109 (1994) 181.

[14] G. Saracco, G. Scibilia, A. Iannibello, G. Baldi, Methane combustion on Mg-doped $LaCrO_3$ perovskite catalysts, Appl. Catal. B: Environ. 8 (1996) 229–244.

[15] G. Saracco, F. Geobaldo, G. Baldi, Methane combustion on Mg-doped $LaMnO_3$ perovskite catalysts, Appl. Catal. B: Environ. 20 (1999) 277–288.

[16] I. Rosso, E. Garrone, F. Geobaldo, B. Onida, G. Saracco, V. Specchia, On the sulphur poisoning of $LaMn_{1-x}Mg_xO_3$ catalysts for natural gas combustion, Appl. Catal. B: Environ., 2000, in press.

[17] D. Trimis, F. Durst, Combustion in a porous medium — advances and applications, Comb. Sci. Technol. 121 (1996) 153–168.

[18] M. Golombok, A. Prothero, L.C. Shirvill, L.M. Small, Surface combustion in metal fibre burners, Comb. Sci. Technol. 77 (1991) 203–233.

[19] B.A. Pint, A.J. Garratt-Reed, L.W. Hobbs, The reactive element effect in commercial ODS FeCrAl alloys, Mater. High. Temp. 13 (1995) 3–16.

[20] V.A. Kazacov, M. Frenklanch, Reduced reaction sets based on GRI-Mech 1.2, University of California at Berkeley, http://www.me.berkeley.edu/drm/.

[21] C.H. Wilke, A viscosity equation for gases mixtures, J. Chem. Phys. 18 (1950) 517.

[22] R.B. Bird, W.E. Steward, E.N. Lightfood, Transport Phenomena, Wiley, New York, 1960.

[23] S. Mathur, P.K. Tondon, S.C. Saxena, Thermal conductivity of binary ternary and quaternary mixtures of rare gases, Mol. Phys. 12 (1967) 569.

[24] J.O. Hirschfelder, C.F. Curtiss, R.B. Bird, Molecular Theory of Gases and Liquids, Wiley, New York, 1954.

[25] R.J. Kee, F.M. Rupley, J.A. Miller, The chemkin thermodynamic data base, Sandia National Laboratories, Report SAND-8215B, 1992.

[26] K.K. Kuo, Principles of Combustion, Wiley, New York, 1986.

[27] E. Tsotsas, H. Martin, Thermal conductivity of packed beds: a review, Chem. Eng. Process. 22 (1987) 19–37.

[28] J.R. Howell, M.J. Hall, J.L. Ellzey, Combustion of hydrocarbons fuels within porous inert media, Prog. Energy Comb. Sci. 22 (1996) 121–145.

[29] R. Viskanta, in: Th.F. Irvine, J.P. Hartnett (Eds.), Advances in Heat Transfer, Vol. 3, Academic Press, New York, 1996, pp. 175–221.

[30] E.M. Sparrow, R.D. Cess, Radiation Heat Transfer, Brooks/Cole Publishing Co., Belmont, CA, 1970.

[31] P.K. Khosla, S.G. Rubin, A diagonal dominant second-order accurate implicit scheme, Comp. Fluids 2 (1974) 207–209.

[32] H. L Stone, Iterative solution of implicit approximations of multi-dimensional differential equations, SIAM J. Num. Anal. 5 (1968) 530–558.

[33] S.V. Patankar, D.B. Spalding, A calculation procedure for heat, mass and momentum transfer in three-dimensional parabolic flows, Int. J. Heat Mass Transfer 15 (1972) 1787–1906.

[34] P.H. Bouma, Methane-air combustion on ceramic foam surface burners, Ph.D. Dissertation, University of Eindhoven, 1997.

[35] Y. Nakamura, Y. Itaya, K. Miyoshi, M. Hasatani, Mechanism of methane–air combustion on the surface of a porous ceramic plate, J. Chem. Eng. Jpn. 26 (1993) 205–211.